

FLIGHT RESULTS FOR THE FORMATION INITIALIZATION AND CONTROL OF THE HE360 PATHFINDER MISSION

Niels H. Roth,^{*} Nathan Cole,[†] Dan CaJacob,[‡] Karan Sarda[§] and Robert E. Zee^{**}

The HE360 Pathfinder mission, successfully launched in December 2018 onboard the SSO-A “SmallSat Express”, is a cluster of three microsatellites that provide independent geolocation of RF signals from space. The geometric diversity required for geolocation is provided through coarse spacecraft formation flying, which seeks to establish and maintain a 125 km along-track offset and 10 km right-ascension offset between the spacecraft. The bulk of the formation initialization phase was completed during the first 6 to 8 weeks of 2019, during which the spacecraft maneuvered from an initially uncontrolled relative separation from the launch vehicle into the nominal formation. The mission is currently in its station-keeping phase, wherein control maneuvers are uploaded to the spacecraft as necessary to maintain the nominal relative configuration with a 1σ accuracy of 5 km. This paper describes the methodology and performance of the formation control algorithms used during the early phases of the HE360 Pathfinder mission.

INTRODUCTION

Formation flying is a key enabling technology for distributed space systems that require control over the relative geometry between spacecraft. This ability to control relative orbital positions is vital for many of the recent and upcoming missions establishing new spaceborne infrastructure for commercial and scientific applications. One commercial application is the geolocation of radio frequency (RF) emitters on Earth using three or more spacecraft. There are a few missions that focus on this application: recently launched HawkEye 360 (HE360) Pathfinder mission and planned constellation;¹ proposed Space Autonomous Mission for Swarming and Geolocating Nanosatellites (SAMSON) technology demonstration;² and upcoming launch of the Kleos Scouting Mission (KSM).

Launched in December 2018 aboard the SSO-A “SmallSat Express”, the HawkEye 360 (HE360) Pathfinder mission uses a cluster of three identical microsatellites flying in formation to demonstrate high-precision geolocation of RF signals. HE360 Pathfinder serves as the first step towards a commercial constellation of satellites that will provide global visualization of RF spectrum usage around Earth.¹ Formation flying technologies developed at UTIAS Space

^{*} GNC Specialist, Space Flight Laboratory, University of Toronto Institute for Aerospace Studies, 4925 Dufferin St., Toronto, Ontario, Canada, M3H 5T6.

[†] MASc. Candidate, Space Flight Laboratory, University of Toronto Institute for Aerospace Studies, 4925 Dufferin St., Toronto, Ontario, Canada, M3H 5T6.

[‡] Director of Space Systems, HawkEye 360, 196 Van Buren St. Suite 450, Herndon, VA, USA, 20170.

[§] Mission Manager, Space Flight Laboratory, University of Toronto Institute for Aerospace Studies, 4925 Dufferin St., Toronto, Ontario, Canada, M3H 5T6.

^{**} Director, Space Flight Laboratory, University of Toronto Institute for Aerospace Studies, 4925 Dufferin St., Toronto, Ontario, Canada, M3H 5T6.

Flight Laboratory (SFL) play a key role in the effective geolocation capabilities of HE360 Pathfinder. Locating the origin of an RF signal requires all three spacecraft to have common ground footprints, offering co-visibility of signals of interest.

Following the successful launch, all three spacecraft deployed from XPOD separation dispensers and made contact with the ground station on their first pass. Platform commissioning was completed between December 4th 2018 and January 11th 2019, and formation initialization began on January 15th 2019. The initialization endpoint was targeted for February 5th 2019, and the formation completed its reconfiguration on February 7th 2019. Despite a few interruptions, formation initialization performed well compared to expectations from simulation, satisfying HE360's mission timeline requirements and making efficient use of propellant thanks to the formation control algorithms. Station-keeping activities began at the conclusion of initialization operations, and continue to effectively maintain formation baselines within their control windows. Presently, formation station-keeping maneuvers are required approximately once a month, resulting in very little down-time for payload operations.

This paper discusses the methodology and performance of the formation control implementation on the HE360 Pathfinder mission during initialization and early station-keeping operations. The spacecraft hardware that enables formation flying is presented, followed by an overview of the mission that motivates this work. Details on the algorithms used for formation initialization, station-keeping, and orbit determination are reviewed before discussing the analysis and results of on-orbit performance. Lastly, there is a brief discussion on the flight experience thus far.

SPACECRAFT OVERVIEW

The HE360 Pathfinder spacecraft, depicted in Figure 1, is based on SFL's proven NEMO bus which has been flown successfully in the GHGSat-D,³ NorSat-1, and NorSat-2 missions.⁴ The spacecraft has dimensions of 20x20x40 cm and a wet mass of approximately 13.4 kg. The primary payload is a software-defined radio (SDR) with a custom RF front-end and a range of antennas to support data collection from VHF to Ku-band.¹ Command and control of the spacecraft is achieved with a low-rate UHF uplink and an S-Band downlink. Payload data downlink is achieved with either S-Band (32 kbps to 2 Mbps) or X-Band (3 to 50 Mbps). There are two onboard computers (OBCs) – a housekeeping computer (HKC) for performing nominal command and data handling such as time-tag script execution, packet routing, and telemetry logging, and a dedicated attitude determination and control computer (ADCC), which performs all attitude sensor data collection and actuation, along with attitude trajectory generation, and attitude/orbit estimation tasks.

Three-axis attitude determination is provided by a set of six fine Sun sensors, a three-axis magnetometer, and a three-axis MEMS rate sensor. Attitude control is provided by a set of three orthogonal reaction wheels complemented with a set of three air-core magnetorquers used for de-tumbling and reaction wheel momentum management. With this hardware set the spacecraft is capable of 5° (2 σ) pointing in sunlight and 10° (2 σ) pointing in eclipse. Orbit determination is provided by a commercial off-the-shelf (COTS) GPS receiver and antenna using GPS-L1 and L2 frequencies. The GPS antenna boresight is oriented along the +Y face of the spacecraft.

Formation control is enabled by an electro-thermal propulsion system. This system uses water as its propellant, so it is safe and easy to fuel. Its power consumption while heating up and thrusting is about 25 W. The nominal thrust level is about 17 mN, though this is configurable through adjusting the tank pressure setpoint via ground command. The specific impulse as tested on the ground is about 175 s. For Pathfinder, the fuel mass is about 750 g, providing an expected Δv of about 98.8 m/s. There is one thrust nozzle located on the -Y face of the spacecraft, such that the spacecraft must be re-oriented for each thrust maneuver.

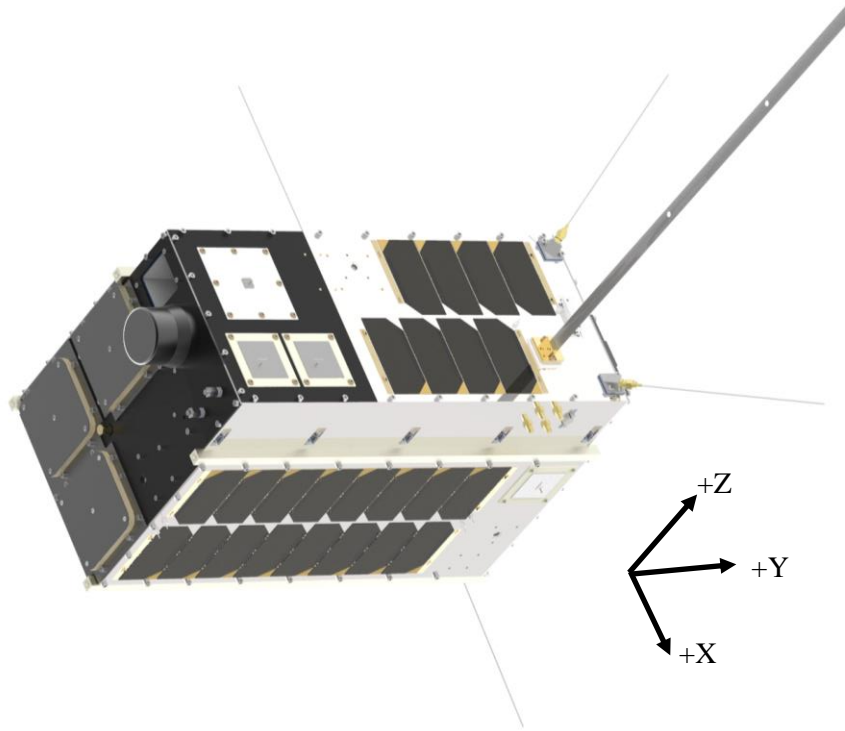


Figure 1. HE360 Pathfinder Spacecraft.

MISSION OVERVIEW

The primary goal of the mission is to demonstrate high-precision RF geolocation from space. To this end, formation keeping is required to maintain a large overlap in the ground footprints of the spacecraft. The target formation has an along-track separation of 125 km between each spacecraft, with a 10 km offset in right-ascension of the ascending node (RAAN) between the middle spacecraft and the leader/follower. This provides a geometric diversity sufficient for target geolocation within the region of interest. The formation control requirements are 5 km (1σ). For this mission only coarse formation keeping is required, since exact relative positioning between spacecraft is not necessary for geolocation – only precise *knowledge* of the relative positions are required. The formation control error is driven primarily by the along-track drift due to offsets in the differential mean semi-major axis resulting primarily from thrust errors and to a lesser extent from differential drag.

All formation control calculations are performed on the ground, uploaded to the spacecraft as “time-tagged” commands by operators, and are executed at the prescribed time by the onboard software. There are several reasons for/advantages of this approach. The major reason is so that the spacecraft is not subject to any limiting export restrictions due to the presence of autonomous formation control technology. Second, this places the burden of software complexity on the ground, where it can be easily modified and updated.

Nominally all spacecraft are in a Sun-pointing attitude, with their maximum solar cell area oriented towards the Sun and the GPS antenna boresight constrained to orbit-normal. The spacecraft can also be programmed to perform ground-target tracking with its S-Band or X-Band antenna in order to maximize data downlink over a ground station or to perform payload data collection.

FORMATION CONTROL ALGORITHMS

The goal of the initialization phase is to design and implement a trajectory that brings the formation from an arbitrary initial relative state, to an arbitrary final desired state, in a fixed

amount of time. This is accomplished in two parts: guidance and control. The guidance law computes a set of intermediate relative orbital states which guide the spacecraft smoothly to the final desired state over a fixed period of time. The control phase uses these intermediate states, or waypoints, and computes a set of maneuvers to achieve the waypoints at the specified time intervals.

In this section we review the main algorithms used for formation initialization, station-keeping, and orbit determination for the HE360 mission. It should be noted that in this work, the relative motion is parameterized using the quasi-non-singular relative orbital elements.⁵

Formation Initialization

The total initialization phase is broken down into two-day sub-intervals (ΔT_{init}), during which roughly 85% of orbits are allotted for control, while 15% are reserved as maneuver-free periods for the purpose of orbit determination used as input for the next initialization window.

The guidance law during formation initialization, or the fuel-optimal reconfiguration from some initial state to a final desired state, is framed as a problem of minimizing the net total change in the differential mean orbital elements.⁵ This is possible since incremental changes in the orbital elements can be equated to impulsive thrust maneuvers (i.e., instantaneous changes in velocity). The guidance plan generates a set of waypoints in differential mean orbital element space from the current time to the desired initialization time in ΔT_{init} intervals. The waypoint at the start of the next sub-interval is used as the target during the current control period.

The set of control maneuvers during each initialization sub-interval is computed using a method which exploits a duality between the continuous and discrete time optimal formation reconfiguration problem in order to iteratively solve for a set of maneuver locations and magnitudes that result in a minimum-fuel maneuver plan to reach the target waypoint at the target time.⁶ This control strategy is augmented to enforce several other constraints on the final solution. First a minimum time-spacing between maneuvers of 45 minutes is applied to limit propulsion system operation for system-level power considerations. Second, configurable “no thrust” windows are specified to prevent maneuvers from being planned inside specific time intervals. This can include thrusting outside ground contact intervals, or only in sunlight to allow for thrust force calibration using ACS data and ensure correct pointing during thrusting, rather than incurring errors due to pointing uncertainty in eclipse. Thrusting in sunlight is also beneficial from a power standpoint – the battery is not drained from these maneuvers. Finally, minimum and maximum Δv /thrust duration bounds are enforced to stay within the operational capabilities of the propulsion system.

Station Keeping

The station keeping guidance law is designed to keep the spacecraft within a designated control window while keeping the spacecraft passively safe using the eccentricity/inclination vector separation concept.⁷ The station keeping phase is conceptualized as a long period of no control (the drift period; approximately 1 week), followed by a short window within which the control maneuvers occur (the control period; approximately 4 orbits). The strategy is motivated by previous work,⁸ whereby during each control window the active spacecraft targets a specific differential semi-major axis which will cause a drift from one side of the control window to the other. Likewise, the relative eccentricity vector is adjusted such that it will be parallel with the relative inclination vector half-way through the drift period, which maximizes safety during the drift period. The relative inclination vector is simply readjusted to its target value during each control period, since there is no drift desired here. The long drift period is allowable because control maneuvers are expected to be infrequent, owing to the fact that all spacecraft will mirror their attitudes thus minimizing the impact of differential drag on the formation. A side-benefit of this strategy is maximizing the time spent performing payload observations.

Formation Control Software

The formation control software is implemented in MATLAB and Systems Tool Kit (STK). A user specifies the spacecraft configuration, final desired formation, constraint options, etc., in a MATLAB configuration file, and provides the initial orbits in STK's ephemeris file format. The main control calculations/optimizations are performed in MATLAB using simplified analytical theories and a relative motion model (state transition matrix) which accounts only for the J_2 perturbation. The resulting control maneuvers are then input to a high fidelity STK/Astrogator simulation to verify that the planned trajectory is executed as expected and that the fuel consumption is acceptable. The software then generates a set of time-tagged command sequences that are directly uploaded to the spacecraft in order to perform the required maneuvers.

Spacecraft Orbit State Estimation

Motivated by previous work,⁹ a full offline orbital state estimation chain was developed for processing the absolute and relative orbits for use in the control algorithms. Each spacecraft's absolute orbit is obtained by first computing single-point solutions based on L1 GPS pseudorange and Doppler observations, and processing these forwards and backwards in time in an EKF. A smoothed coarse estimate is then obtained as an inverse-covariance weighted sum of the forwards and backwards solutions. These "coarse" estimates are then used to evaluate the expected measurement equations and remove outlier pseudorange and carrier phase observations in a statistical data editing process. Measurements are further filtered based on a minimum antenna to GPS satellite elevation angle and a minimum C/N_0 . The edited measurements then go through an optional measurement combination step where the GRAPHIC¹⁰ or L1/L2 ionosphere-free (IF) observations are formed. Finally, the remaining raw measurements are used to in an EKF/smoother to obtain a "fine" absolute state estimate. The relative state estimate is obtained by using one of the fine absolute states as a reference, and processing single-difference (SD) pseudorange and SD carrier phase, or SD IF observables in an EKF/smoother using pseudo-relative orbital dynamics.⁹ The nominal GPS data period for the above filtering is 30 s. The appropriate mappings between the antenna phase centre and spacecraft centre of mass are accounted for using onboard attitude solutions recorded at the same data period. The GPS satellite orbits can be taken from either broadcast ephemeris, or published SP3 files containing the ultra-rapid, rapid, or final GPS satellite orbits. Low rate GPS satellite clock data from the standard SP3 file is used (i.e., 15 minute period), and coordinate transformations between J2000 and ECEF are performed using linearly interpolated EOP at the time of interest. The modelled orbital dynamics include a 70x70 EGM2008 gravity model, third body perturbations due to Sun and Moon, atmospheric drag using a Harris-Priester density model, and solar radiation pressure.

While the aforementioned filters were originally designed and implemented for operational use in the MATLAB environment, in practice they were found to be too slow for use in real time – it was not possible to process the orbits, run the initialization controller, and to prepare the time-tag command scripts for operators to upload within a one-orbit period between satellite contacts.

As such, for orbital operations a simplified method was used for obtaining absolute and relative mean orbital elements for input to the formation control algorithms. Position and velocity estimates from the GPS receiver recorded at a 30 s period are filtered using the same "coarse" procedure as above. A 30x30 gravity model is used for propagation, as this was found to be sufficient for obtaining smooth estimates – drag, higher order gravitational terms, third body effects, solar radiation pressure, etc., are all omitted from the simple model, which favours execution speed over accuracy.

The absolute orbits are then input to STK, where they are converted to Brouwer mean orbital elements with the short period oscillations removed, and expressed in the True-of-Date (TOD) reference frame. The True-of-Date mean orbital elements are used in the averaging procedure

rather than the J2000 elements to avoid large variations in the mean elements over time due to the impact of the Earth's precession and nutation on the period and amplitude of the long-periodic oscillations in the orbital elements.¹¹ Finally, numerical averaging over a period of four orbits is used to obtain the initial mean orbital elements input to the formation control algorithms.

FORMATION INITIALIZATION RESULTS

The spacecraft were deployed into a circular Sun-synchronous orbit (SSO) at an altitude of about 590 km, with a 10:30 local time of descending node (LTDN). The spacecraft were separated from the launch vehicle at five-minute intervals with uncontrolled and unknown relative orientations, using SFL's XPOD deployment system. Based on the XPOD spring design, each spacecraft's deployment velocity was expected to be about 1.7 m/s. All three spacecraft were contacted during the first pass over the HE360 ground station in Herndon, VA roughly 7.5 hours after launch. After verifying safe spacecraft temperatures and health of the spacecraft power system, the main housekeeping computer (HKC) application was loaded and the GPS receivers were powered on. The initial absolute and relative orbital elements based on the earliest-available GPS data are summarized in Table 1. Based on examination of the initial relative orbits, it was decided that Hawk-A would be the leading spacecraft in formation, Hawk-C would be the middle spacecraft with the RAAN offset, and Hawk-B would be the trailing spacecraft. This configuration was selected for two main reasons. First, it would be the safest to establish, not requiring the spacecraft to cross each other in the along-track direction. Second, Hawk-C already had a 500 m offset in its differential inclination following deployment and thus would require the least amount of fuel to reach the final desired configuration as the natural relative motion in the weeks leading up to the first thrusts would increase its relative RAAN towards 10 km at no additional effort.

Table 1. Initial mean orbital elements for Hawk-A, and relative mean orbital elements for Hawk-B (ref) and Hawk-C (ref) after separation from the launch vehicle – Epoch 2018-12-04 10:07:42 UTC.

	a (km)	e (-)	i (°)	Ω (°)	$u = \omega + f$ (°)	
Hawk-A	6954.554	2.5×10^{-4}	97.7687	47.569	6.92042	
	δa (km)	$\delta \lambda$ (km)	δe_x (km)	δe_y (km)	δi_x (km)	δi_y (km)
Hawk-B	-1.24	96.35	0.196	-1.73	-0.081	0.244
Hawk-C	-0.786	62.2	0.242	-1.59	0.506	-0.178

The final desired configuration in terms of relative mean orbital elements is given in Table 2. Note that the controlled spacecraft are used as the reference spacecraft. This is done so that when solving for the maneuver locations, the time/position in orbit is expressed in terms of the spacecraft applying the thrust rather than a reference spacecraft thousands of kilometres away.

Table 2. Desired Relative Mean Orbital Elements – Controlled Spacecraft as Reference.

	δa (km)	$\delta \lambda$ (km)	δe_x (km)	δe_y (km)	δi_x (km)	δi_y (km)
Hawk-B	0	250	0	0	0	0
Hawk-C	0	125	0	0	0	10

The next two weeks of the guidance, navigation, and control system commissioning were spent assessing the GPS performance, ensuring smooth operation of the data processing tools on the ground, and testing, tuning, and verifying the spacecraft pointing performance in their

nominal Sun-pointing attitude as well as in ground target-tracking for optimizing data down-link. During this period it was observed that the spacecraft pointing error in eclipse was larger than expected, as inferred from the magnitude of attitude correction upon transition from eclipse to sunlight. In order to not further delay formation initialization, it was decided to apply a “no thrusting in eclipse” constraint to the initialization maneuvers. This was to ensure that no time/fuel was wasted due to large thruster pointing errors causing unwanted changes in the relative trajectory.

Propulsion system commissioning began on December 20th and 21st, 2018. A set of manual along-track maneuvers ranging in duration from 5 s to 45 s were uploaded to the three spacecraft in order to compute thrust magnitude estimates and to calibrate the thrust feed-forward torque applied by the attitude control system to ensure correct pointing during long-duration thrusts. Along-track thrusts were selected because they would help arrest the relative motion to minimize fuel consumed during formation initialization.

Thrust force calibration was performed by offline processing of attitude telemetry collected at 1 Hz during the calibration maneuvers. Using fine Sun sensor and magnetometer telemetry, the TRIAD algorithm was used to estimate a set of attitude quaternions. The TRIAD estimates were then smoothed using a simple averaging method, and the spacecraft angular rate and accelerations were obtained from finite differencing. Then, combined with knowledge of the spacecraft inertia, reaction wheel speeds, commanded reaction wheel and magnetorquer torques, along with environmental disturbance torques, the dynamic equations of motion were inverted to solve for the thrust disturbance torque during each maneuver. This disturbance torque was averaged over the thrust time period and then divided by the moment arm (based on the spacecraft solid model) to yield a thrust force estimate.

The thrust force for the propulsion system is heavily dependent on the tank pressure and temperature. The propellant tank has a heater, which can be used to regulate the tank to a known temperature/pressure setpoint. Early on, only a temperature setpoint could be commanded and it was observed that the controller did a poor job of regulating the tank pressure in this manner. As a result, it was decided to keep the tank heater disabled and to rely on the ± 1 °C steady-state tank temperature variation throughout the orbit. In this condition, the thrust magnitude was found to be approximately 14.5 mN on all three spacecraft. This value was used in all subsequent formation initialization operations.

Table 3. Formation Initialization Timeline.

Date (UTC)	Comment
2018-12-03	Mission launched.
2018-12-04 to 2018-12-19	Guidance, navigation, control system commissioning; attitude control system tuning; preparation for first thrusts.
2018-12-20 to 2018-12-22	First thrusts on Hawk-A, Hawk-B, and Hawk-C.
2018-12-23 to 2019-01-07	No commissioning activities due to University closure for holidays.
2019-01-08 to 2019-01-14	Completion of thrust magnitude calibration and tuning of attitude performance during thrusts for all spacecraft.
2019-01-15	Formation initialization maneuver sequences begin for Hawk-B and Hawk-C; initialization endpoint 2019-02-05.
2019-02-07	Formation initialization complete.

The full timeline of formation initialization from launch is provided in Table 3. After completing the thrust calibration maneuvers, just over three weeks were required to fully initialize the formation from the initial conditions shown in Table 4 to the final desired formation in

Table 2. The full relative trajectory from launch to initialization for Hawk-C relative to Hawk-A is shown in Figure 2 (in-plane motion) and Figure 3 (in-plane oscillation and out of plane motion).

Table 4: Initial mean orbital elements for Hawk-A, and relative mean orbital elements for Hawk-B (ref) and Hawk-C (ref) at start of initialization – Epoch 2019-01-15 12:10:42 UTC.

	a (km)	e (-)	i ($^{\circ}$)	Ω ($^{\circ}$)	$u = \omega + f$ ($^{\circ}$)	
Hawk-A	6954.655	2.59×10^{-3}	97.7618	89.29	72.0	
	δa (km)	$\delta \lambda$ (km)	δe_x (km)	δe_y (km)	δi_x (km)	δi_y (km)
Hawk-B	-0.211	5849.29	-1.55	1.46	-0.182	2.13
Hawk-C	0.194	3775.69	-1.33	1.06	0.365	3.91

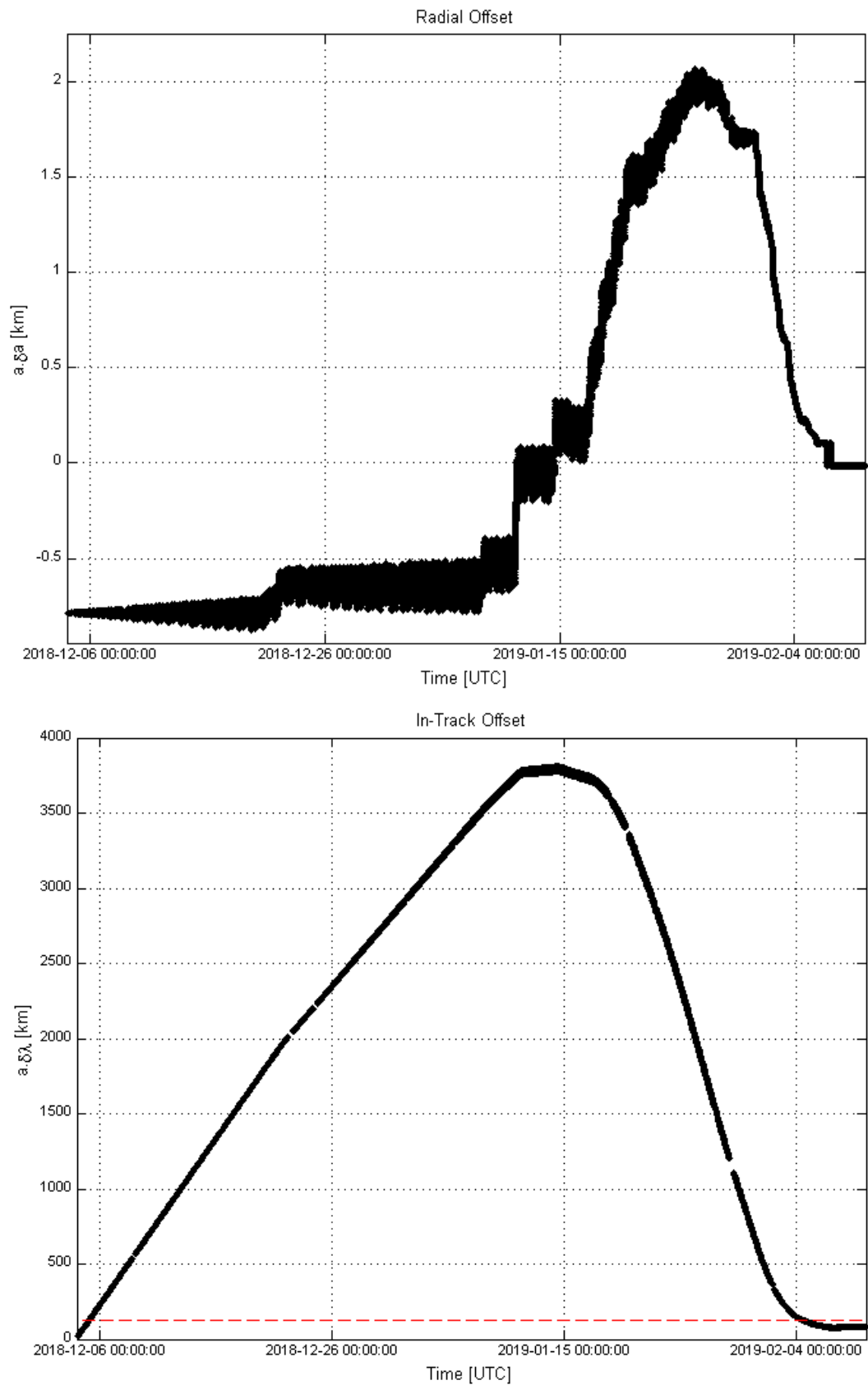


Figure 2. Hawk-C (ref) and Hawk-A, relative semi-major axis and mean argument of latitude during formation initialization, from on-orbit GPS data.

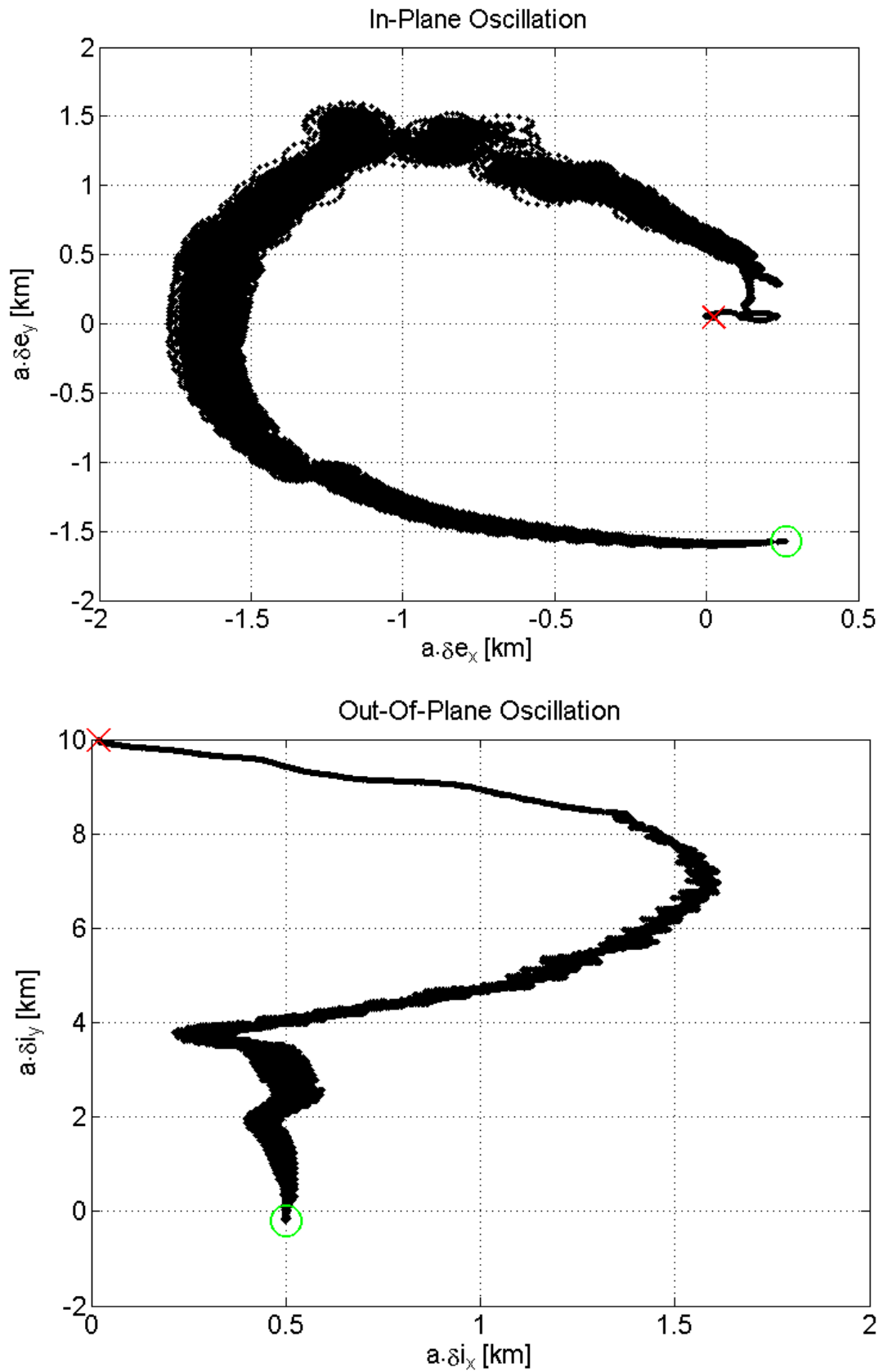


Figure 3. Hawk-C (ref) and Hawk-A, relative eccentricity and inclination vector during formation initialization, from on-orbit GPS data.

Initialization Delta-V

In this section we discuss the fuel cost of the formation initialization maneuver plan. Comparisons are made between the actual (on-orbit) Δv and the expected Δv from simulated a priori maneuver plans. As a figure of merit, Δv costs are compared to a lower bound that represents the theoretical minimum Δv required to perform any formation reconfiguration over a finite time period using a simple two-thrust maneuver while leveraging the natural relative motion dynamics between the two maneuvers.

Table 5. Constraints Applied to Formation Initialization Control Algorithm.

Initialization deadline	February 7, 2019
Open-loop control period	2 days
Minimum time between maneuvers	45 minutes
Maneuver-free orbit determination period	4 orbits
Thrusts location restrictions	Eclipses Ground station passes Orbit determination periods
Thrust magnitude	14.5 mN
Minimum impulse	50 mNs
Maximum impulse	870 mNs

From Table 4, formation initialization officially began on January 15th 2019, following the conclusion of commissioning activities for attitude control system tuning and propulsion system calibration. An initialization maneuver plan was computed for a reconfiguration interval of 15 Jan 2019 16:15:00.00 UTC to Feb 4 2019 23:00:00.000 UTC. Referring to Table 5, this initialization plan was constrained to thrust only in sunlight and to have a minimum time between thrusts of 45 minutes. Formation initialization control periods were nominally set for consecutive two day intervals, with maneuver-free orbit determination arcs specified immediately following each intermediate waypoint. The propulsion system was limited to a maximum impulse of 870 mNs and a minimum impulse of 50 mNs.

The maneuver plan in Figure 4 represents open-loop control of the Hawk-C/Hawk-A formation pair based on initial conditions from an orbit determination solution prior to the initialization epoch time (see Table 4). This first iteration of the maneuver plan provides an expected reconfiguration cost of using the formation initialization control implementation. It uses the relative motion model and high fidelity orbit propagation environment of STK to simulate the entire initialization trajectory. Each control period is simulated using operational parameters, with position and velocity reports from STK providing pseudo closed-loop feedback as the simulation progresses through its initialization trajectory. Unlike ground testing, the flight algorithm does not attempt to model any navigation or control uncertainty – unmodeled dynamics are the primary source of error in the open-loop initialization plan. This open-loop maneuver plan emulates a perfect execution of formation initialization assuming no interruptions or complications arise during formation flying operations. In the ideal case, minor deviations due to control, estimation, and modelling errors do not manifest as significant differences in total Δv .

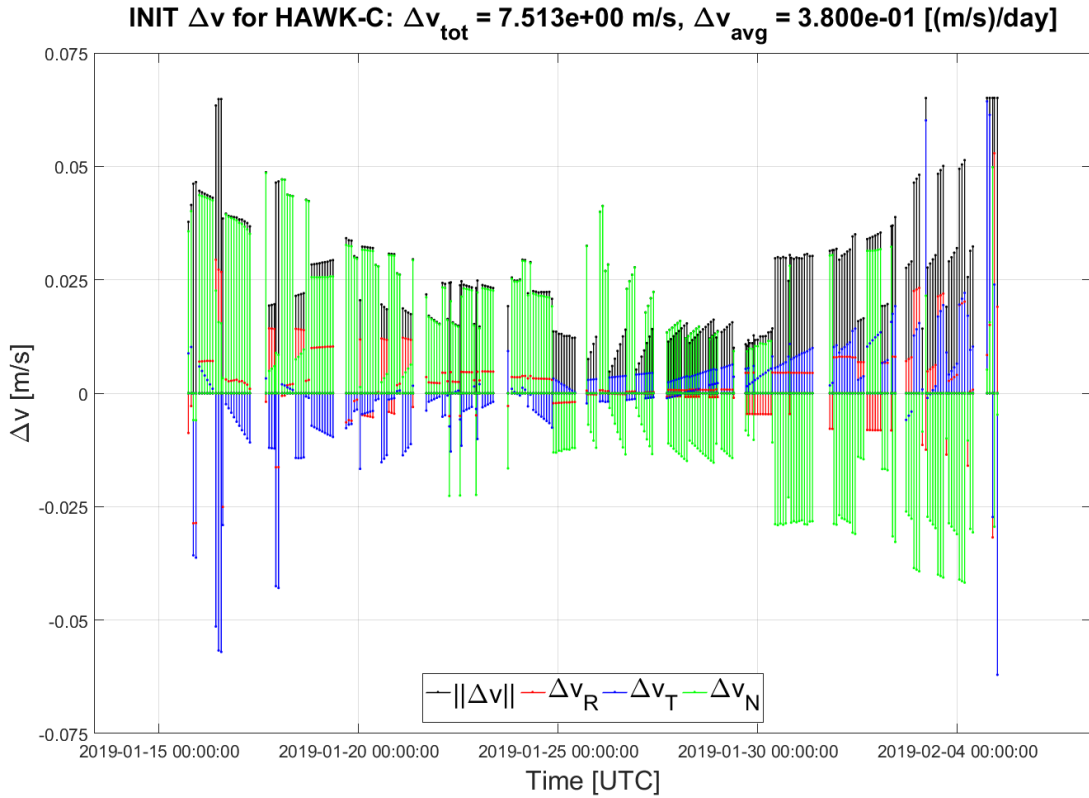


Figure 4. Maneuver plan of entire open-loop initialization sequence for Hawk-C representing the Δv components of each impulsive thrust.

To evaluate how achievable a reconfiguration plan is, the magnitude and Δv components of each thrust, as well as the general shape of the maneuver sequence, is considered. The open-loop maneuver plan in Figure 4 exemplifies an acceptable solution, meaning the proposed initialization scenario is achievable within operational constraints imposed on the formation. There are few maximum Δv maneuvers, which indicates the fixed-time reconfiguration period is long enough, and the required total relative orbital element (ROE) variations are small enough, to be realized by the propulsion system capabilities. Specifically, only 9 of the 290 thrusts that were planned have the maximum Δv of ~ 0.065 m/s, which was imposed to keep the duration of impulsive thrusts below 60 seconds – the maximum thrust duration specified by the manufacturer. There are also few minimum Δv maneuvers, indicating the propulsion system’s control authority over the instantaneous ROE variations is achievable. Specifically, the minimum Δv that can be reliably expected of the propulsion system is ~ 0.004 m/s, which dictates the smallest realizable ROE variation with a single thrust. Considering the general division of Δv components over the full plan, we observe that maneuvers are dominated by tangential and normal thrusts. This agrees with the required variation in ROEs that Hawk-C needs to achieve during initialization (compare Table 4 with Table 2). Additionally, the trend of large tangential and normal maneuvers in opposite directions at the beginning and end of the sequence maximizes the leverage of natural drift during reconfiguration. These thrusts are used to affect variation in along-track and cross-track formation baselines, $\Delta\delta\lambda$ and $\Delta\delta i_y$, respectively.

The original operational plan was to update the initial open-loop maneuver plan, shown in Figure 4, with regular orbit determination solutions. Thus, incrementally revising the overall maneuver plan in a closed-loop to account for unmodeled dynamics and control error during the commanded thrust sequences. In this way, only thrusts for a single control period are commanded open-loop, with the planning of each subsequent control period accounting for the ROE variations introduced during the segment preceding it. A slightly revised set of maneuvers are

uploaded to the satellites before each control period without any disruption in the overall thrust sequence.

However, in reality there were operational complications involving unsuccessful thrusts, poor orbit determination solutions, and missed communication windows that impacted this process. These complications resulted in deviations from the original trajectory, due to unplanned formation drift, that require new maneuver plans to be computed after each interruption. Therefore, the actual initialization sequence followed a piecewise trajectory, as a consequence of combining multiple maneuver plans instead of following the original plan exactly – this piecewise trajectory is illustrated by Figure 2 and Figure 3.

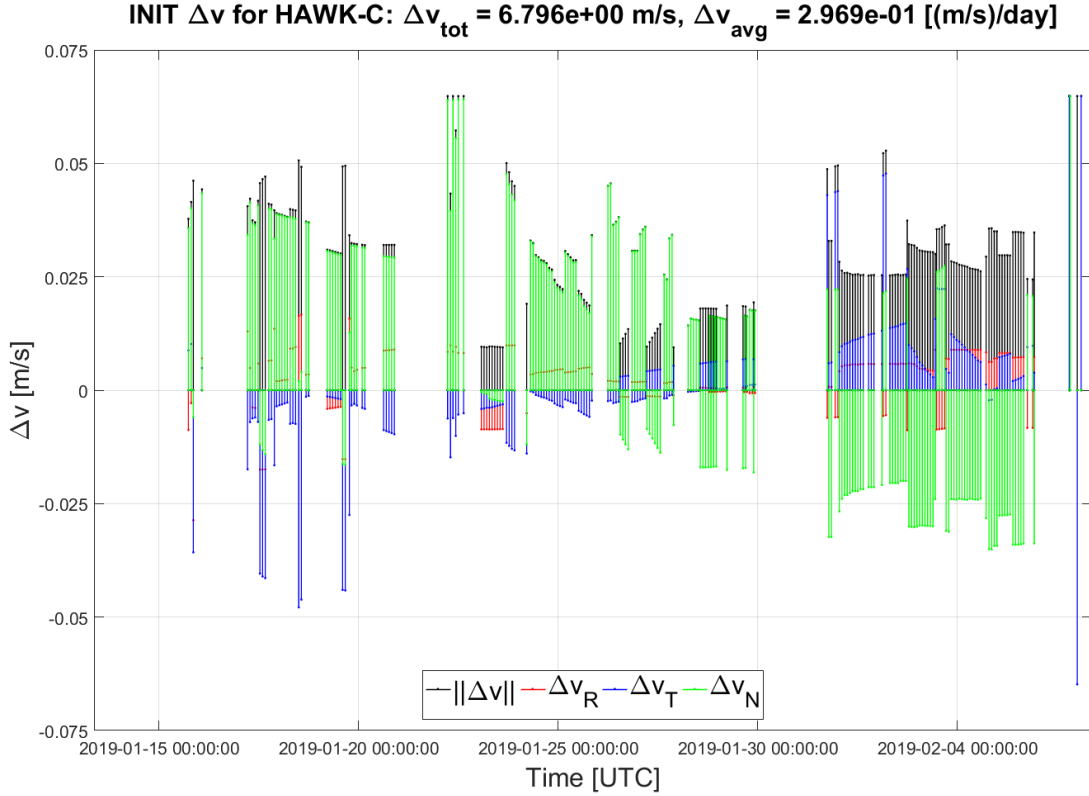


Figure 5. Actual piecewise maneuver plan executed during initialization sequence for Hawk-C representing the Δv components of each impulsive thrust.

The composite maneuver plan in Figure 5 corresponds to the piecewise initialization trajectory. Comparing this to the open-loop initialization trajectory in Figure 4, there are both similarities and differences to note. First, it is apparent that there are various gaps within the actual trajectory that do not align with the regular maneuver-free periods found in the planned sequence. These gaps in the maneuver sequence were caused by various interruptions to nominal formation reconfiguration operations. Each interruption resulted in deviations from the planned trajectory, which required new maneuver plans that took this formation drift into account. As opposed to the ten maneuver-free periods (reserved for orbit determination) that were planned during the open-loop initialization sequence, the actual sequence only had four – the entire reconfiguration was carried out using five open-loop thrust sequences. For Hawk-C, these sequences were comprised of up to 98 consecutive open-loop thrusts. Due to the long duration of these open-loop sequences, the final sequence of four maneuvers required large thrusts to account for compounded error from so many consecutive thrusts. It should also be noted that the final initialization segment switched to the station-keeping control algorithm, using one normal thrust and three tangential thrusts to accomplish the final reconfiguration of Hawk-C.

A comparison of the actual number of thrusts and corresponding Δv cost is summarized in Table 6. The difference between expected and actual Δv , and corresponding reduction in number of thrusts, is a consequence of extending the initialization endpoint and using multiple re-configuration epochs in the piecewise initialization plan. Shifting the fixed-time initialization endpoint by two days, to February 7th, compensated for time lost and unplanned drift incurred during interruptions of maneuver operations. Referring to Table 6, there was a smaller performance difference between planned and actual initialization for Hawk-B (98.6% of expected Δv , 87.6% of planned thrusts) compared to Hawk-C (90.5% of expected Δv , 77.2% of planned thrusts). This is attributed to a series of maximum duration tangential thrusts that were manually commanded on Hawk-B, in addition to the shifted epoch and endpoint times having less impact on the formation pair that was not establishing a large RAAN offset. The manual maneuvers, although not fully optimized for Δv , were necessary to slow down the along-track rendezvous of Hawk-B with its planned separation from Hawk-A. This was an operational decision to mitigate overshoot.

Table 6. Number of thrusts and Δv cost for planned and actual maneuver sequences, along with theoretical minimum Δv required to accomplish total ROE variation.

	Planned Thrusts	Expected Δv (m/s)	Actual Thrusts	Actual Δv (m/s)	Δv Lower Bound (m/s)
Hawk-B	225	5.12	197	5.05	2.87
Hawk-C	290	7.51	224	6.80	4.65

Extending the initialization period and shifting epoch times, and consequently shifting intermediate waypoint times, had a larger impact on Hawk-C, which was establishing in-plane and out-of-plane formation baselines. It has been noted that the formation initialization control algorithm is sensitive to epoch time and duration of the fixed-time reconfiguration period. As such, one optimal maneuver plan can be significantly more costly than another that has slightly shifted epoch and endpoint times. This issue may be more evident when optimizing over longer intermediate waypoint intervals, such as the two day control periods used for this mission – to the authors’ knowledge, literature has primarily considered intervals durations on the order of a few orbits.⁶ Having fixed-time waypoints with long intervals between them is a further restriction on where control maneuvers can be placed within a minimum-fuel plan. Longer open-loop maneuver sequences also amplify unmodeled effects from ROE variations introduced by commanding more sequential thrusts.

To evaluate reconfiguration maneuver plan optimality, it can be compared to the analytical Δv lower bound, Δv_{LB} . This figure of merit represents an estimate for the minimum Δv required to achieve any reconfiguration. Due to the ROE parameterization used, instantaneous in-plane and out-of-plane variations produced by tangential and normal thrusts are decoupled from one another and can be considered independently.¹² However, the time-evolution of ROEs is not decoupled unless some small contributions from first-order J_2 effects are neglected.¹³ To estimate cost of the total in-plane ROE variation, the largest contributor from the following can be considered: changing the size of the relative orbit by instantaneously modifying the relative eccentricity vector magnitude, $\|\Delta\delta\mathbf{e}\|$, with a single tangential maneuver at the necessary phase angle; arresting drift by zeroing the relative semi-major axis, $|\Delta\delta a|$, with a pair of tangential maneuvers; or modifying the along-track separation by leveraging drift in the relative mean longitude, $|\Delta\delta\lambda|$, with a pair of tangential maneuvers.¹² The third contributor is a subset of the second, since it induces the desired variation in $\delta\lambda$ by means of a $\Delta\delta a$ – that is, a pair of maneuvers that first establish some $\delta a = \delta a_{transf}$ for drift and then bring $\delta a = 0$ to arrest any further along-track drift. Additionally, an assumption is made that all in-plane variations can be accomplished with two thrusts by placing tangential maneuvers at the necessary phase angle to achieve the required $\Delta\delta\mathbf{e}$. This same approach is extended for total out-of-plane variation,

by considering the minimum of: instantaneous variation of the inclination vector, $\|\Delta\delta\mathbf{i}\|$, with a single normal thrust at the necessary phase angle; or modifying the cross-track separation by leveraging drift in the differential RAAN, $\Delta\delta i_y$, with a pair of normal thrusts placed to adjust the differential inclination, δi_x .

Table 7. Analytical estimate of minimum Δv required to achieve total in-plane and out-of-plane ROE variations for Hawk-C based on initial conditions.

	In-Plane	Out-of-Plane
Total Instantaneous Variation (km)	$\Delta\delta a = 2.126$	$\Delta\delta i_x = 4.134$
Total Variation from Drift (km)	$\Delta\delta\lambda = 3612.485$	$\Delta\delta i_y = 4.497$
Δv Lower Bound (m/s)	1.16	4.50

Table 7 summarizes the Δv lower bound results for Hawk-C based on the initial conditions from Table 4 and the desired ROE state in Table 2. Note that Δv_{LB} presented in Table 7 does not account for any coupling between in-plane and out-of-plane dynamics. The totals summarized in Table 6 represent two-thrust maneuvers with tangential and normal components that combine all in-plane and out-of-plane variations. This estimate also does not consider any hardware limitations of the spacecraft, such as maximum impulse of the propulsion system. This lower bound also disregards any operational limitations, such as thrusts being restricted to sunlit portions of the orbit only. All of these factors contribute to the Δv lower bound that is actually achievable on-orbit. Refer to Table 6 for a comparison between the expected and actual Δv cost, and the estimated Δv lower bound for total ROE variation. In both cases the theoretical limit is about 2.2 m/s lower than the actual fuel used. This result is thought to be quite good, considering the limitations of the physical system as compared to perfectly impulsive thrust pairs. Overall, the fuel margin for the mission is very high, having used about 5% (Hawk-B) and 7% (Hawk-C) of the total available fuel for initialization.

STATION KEEPING RESULTS

Since entering the station-keeping (SK) phase of the mission, there have been two notable differences from the pre-launch plan. The changes were made in order to maximize up-time of the operational mission and to minimize fuel use even further. First, the original notion was to perform SK maneuvers on a fixed weekly schedule. This results in a downtime of approximately 4 orbits per week, since both the propulsion system and primary payload cannot be operated simultaneously due to power restrictions. Operationally, the SK maneuvers have been performed on as-needed basis, as dictated by when the along-track control error is predicted to exceed roughly 15 km. To date, this has typically been a single short-duration maneuver to raise or lower the orbits on the order of 5 m in order to change the direction of the relative motion. The impact of these thrusts on the relative eccentricity vector are neglected, since the impact on the overall in-plane control error is small. Similarly, maintenance on the uncoupled out-of-plane motion (i.e., relative inclination vector control) is scheduled when the error is projected to exceed roughly 40 m, which can be corrected with a single long-duration thrust in the orbit-normal direction.

The second major change was the decision to altogether omit SK thrusts to control the relative eccentricity vector. This is justified because following initialization, the relative eccentricity vectors have a magnitude of about 50 m, and an in-plane oscillation of this magnitude does not impact geolocation activities. Operational safety through appropriate phasing of the relative eccentricity and inclination vectors is not of concern here, since safety is ensured through the 125 km along-track baseline. The omission of these maneuvers also means less operational down-time.

Overall, the revised in-plane control method results in a two-fold fuel savings. First, no fuel is needed to correct the relative eccentricity vector – it is allowed to drift freely. Second, no additional fuel is required to correct the in-plane and out-of-plane motion errors induced by thrust errors during these eccentricity corrections (e.g., location in the orbit, orientation with respect to the local orbital frame, magnitude errors).

At present, the state of the formation is passively monitored by operators, and maneuvers are manually planned and scheduled around operational activities. This eases the operational burden, since the maneuver frequency is on the order of months rather than at a fixed weekly cadence. The relative motion from the SK phase of the mission (Feb. 7 2019 to May 24 2019) is shown in Figure 6. In this timespan, there have been 5 SK maneuvers for Hawk-C (Δv of 0.059 m/s) and 5 SK maneuvers for Hawk-B (Δv of 0.093 m/s). The Hawk-B fuel use is a little higher due to application of one out-of-plane (OOP) SK thrust, whereas no OOP correction has yet been applied to Hawk-C. These are much lower than the 0.45 m/s (0.03 m/s/week) that was originally budgeted for SK operations. The difference is due to the aforementioned operational changes.

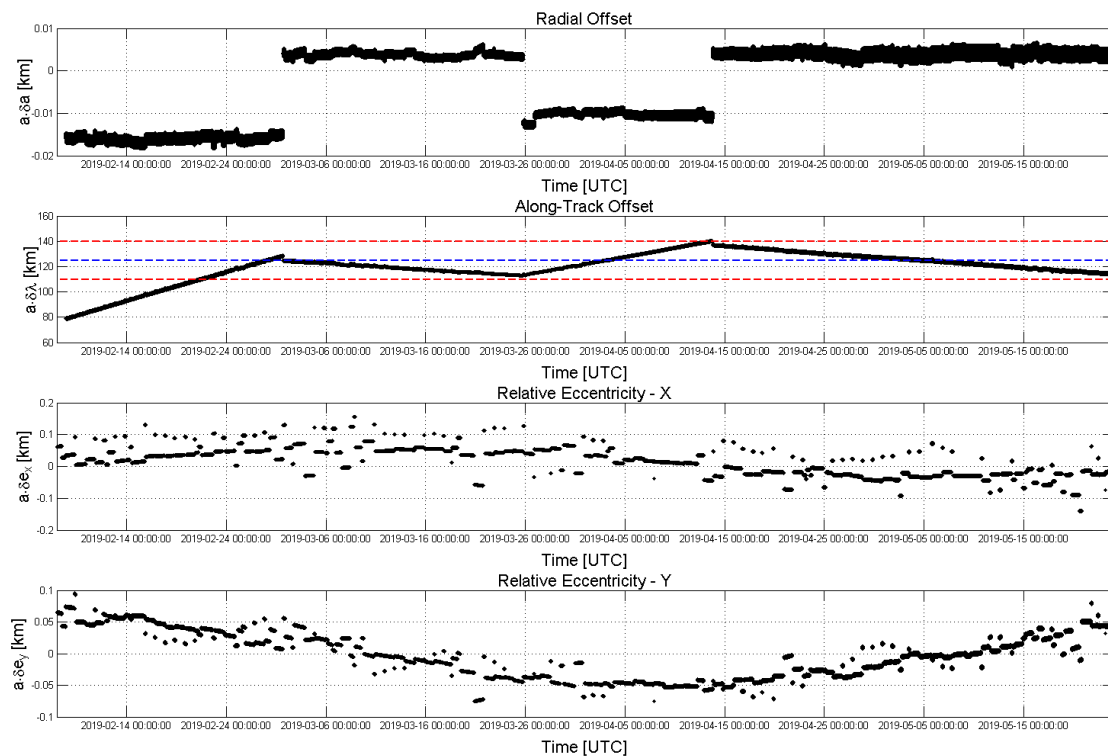


Figure 6. Hawk-C (ref) and Hawk-A, relative in-plane motion during station-keeping, from TLE data.

CONCLUSION

Following the successful launch and platform commissioning of the HE360 Pathfinder mission from early December 2018 to mid-January 2019, the target formation was successfully achieved in just over three weeks using five sets of openloop thrust sequences uploaded to the Hawk-B and Hawk-C spacecraft. The fuel required compares well with the theoretical minimum fuel for the same reconfiguration with idealized changes in velocity. A very healthy fuel margin is maintained following initialization, with more than 93% of the available Δv remaining (per spacecraft). This excellent result demonstrates the utility and success of the guidance and control algorithms employed during this phase of the mission, in addition to showing outstanding performance and reliability of the spacecraft themselves during the high-maneuvering phase of the mission. At present the spacecraft are in the station-keeping phase, performing

minor corrective maneuvers every 3 to 6 weeks (as needed) in order to maintain the nominal relative configuration. Here too the spacecraft maintain very high fuel margins, owing to a more relaxed pace of station-keeping operations than originally envisioned. The success of the formation control has facilitated payload commissioning and operations, and nominal commercial operations are now underway.

ACKNOWLEDGMENTS

The authors would like to thank the teams of engineers, managers and support personnel at the offices of HawkEye 360, Deep Space Industries, GomSpace, and Space Flight Laboratory who devoted their time and passion in enabling this project to take shape.

REFERENCES

- [1] Daniel CaJacob, Nicholas McCarthy, Timothy O’Shea, and Robert McGwier, “Geolocation of RF Emitters with a Formation-Flying Cluster of Three Microsatellites”, in *Proc. of 30th Annual AIAA/USU Conference on Small Satellites (SmallSat 2016)*, Logan, Utah, USA, August 2016.
- [2] A. Kaidar et al., “GPS Disciplined Oscillator for Geolocation with the Samson Satellite Cluster,” in *Proc. Of 5th Federated and Fractionated Satellite Systems Workshop (FSS 2017)*, Toulouse, France, November 2017.
- [3] N. Ibrahim et al., “On-Orbit Earth Observation Performance of GHGSat-D”, in *Proc. of 11th IAA Symposium on Small Satellites for Earth Observation*, Berlin, Germany, April 2017.
- [4] J. Harr et al., “Microsatellites for Maritime Surveillance – an update on the Norwegian Smallsat Program”, in *Proc. of 69th International Astronautical Congress (IAC)*, Bremen, Germany, October 2018.
- [5] G. Gaias, S. D’Amico, and J.S. Ardaens, “Generalized Multi-Impulsive Maneuvers for Optimum Spacecraft Rendezvous”, in *Proc. of 5th International Conference on Spacecraft Formation Flying Missions and Technologies (SFFMT 2015)*, Munich, Germany, May 2013.
- [6] C. W. T. Roscoe, J. J. Westphal, J. D. Griesbach, and H. Schaub, “Formation Establishment and Reconfiguration Using Differential Elements in J_2 -Perturbed Orbits”, *Jour. of Guidance, Control, and Dynamics*, Vol. 38, No. 9, pp. 1725-1740, Sept. 2015.
- [7] S. D’Amico and O. Montenbruck, “Proximity Operations of Formation-Flying Spacecraft Using an Eccentricity/Inclination Vector Separation”, *Jour. of Guidance, Control, and Dynamics*, Vol. 29, No. 3, pp. 554-563, May-June 2006.
- [8] S. D’Amico, *Autonomous Formation Flying in Low Earth Orbit*, PhD thesis, TU Delft, 2010.
- [9] R. Kroes, “Precise relative positioning of formation flying spacecraft using GPS,” Tech. Rep 61, Netherlands Geodetic Commission, March 2006.
- [10] S. Leung and O. Montenbruck, “Real-time navigation of formation-flying spacecraft using global-positioning-system measurements,” *Jour. of Guidance, Control, and Dynamics*, vol. 28, pp. 226-235, March-April 2005.
- [11] Weichao Zhong and Pini Gurfil, “Mean Orbital Elements Estimation for Autonomous Satellite Guidance and Orbit Control,” *Journal of Guidance, Control, and Dynamics*, Vol. 36, No. 6, Nov-Dec, 2013, pp. 1624-1641.

- [12] G. Gaias and S. D'Amico, "Impulsive Maneuvers for Formation Reconfiguration Using Relative Orbital Elements," *Jour. of Guidance, Control and Dynamics*, Vol. 38, No. 6, pp. 1036-1049, June 2015.
- [13] M. Chernick, S. D'Amico, "New Closed-Form Solutions for Optimal Impulsive Control of Spacecraft Relative Motion," *Jour. of Guidance, Control, and Dynamics*, vol. 41, pp. 301-319, February 2018.